

# 000 NEUROACOUSTIC PATTERNS: CONSTANT Q CEP- 001 STRAL COEFFICIENTS FOR THE CLASSIFICATION OF 002 NEURODEGENERATIVE DISORDERS 003

004 **Anonymous authors**  
 005  
 006

007 Paper under double-blind review  
 008  
 009

## 010 ABSTRACT 011

012 Early identification of neurodegenerative diseases is crucial for effective diagno-  
 013 sis in neurological disorders. However, the quasi-periodic nature of vocal tract  
 014 sampling often results in inadequate spectral resolution in traditional spectral fea-  
 015 tures, such as Mel Frequency Cepstral Coefficients (MFCC), thereby limiting their  
 016 classification effectiveness. In this study, we propose the use of Constant Q Cep-  
 017 stral Coefficients (CQCC), which leverage geometrically spaced frequency bins  
 018 to provide superior spectrotemporal resolution, particularly for capturing the fun-  
 019 damental frequency and its harmonics in speech signals associated with neurode-  
 020 generative disorders. Our results demonstrate that CQCC, when integrated with  
 021 Random Forest and Support Vector Machine classifiers, significantly outperform  
 022 MFCC, achieving absolute improvements of 5.6 % and 7.7 %, respectively. Fur-  
 023 thermore, CQCC show enhanced performance over traditional acoustic measures,  
 024 such as Jitter, Shimmer, and Teager Energy. The effectiveness of CQCC is un-  
 025 derpinned by the form-invariance property of the Constant Q Transform (CQT),  
 026 which ensures consistent feature representation across varying pitch and tonal con-  
 027 ditions, thereby enhancing classification robustness. Furthermore, the robustness  
 028 of CQCC features against MFCC features are validated using LDA plots. These  
 029 findings are validated using the Italian Parkinson’s database and the Minsk2019  
 030 database of Amyotrophic Lateral Sclerosis, underscoring the potential of CQCC  
 031 to advance the classification of neurodegenerative disorders.  
 032

## 033 1 INTRODUCTION 034

035 Neurodegenerative disorders have become a significant and escalating health concern as popula-  
 036 tions age globally. These disorders are marked by the gradual loss of neuronal function, leading to  
 037 debilitating cognitive and motor impairments. Despite the availability of advanced medical tech-  
 038 nologies, diagnosing and managing these diseases remain significant challenges. The complexities  
 039 of these conditions, coupled with the limitations of current therapies, emphasize the urgent need for  
 040 innovative approaches to both diagnosis and treatment.

041 Neurodegeneration stands out as the central pathological process in the majority of brain-related  
 042 conditions (Jeong et al., 2024). Conditions like Parkinson’s Disease (PD) and Amyotrophic Lateral  
 043 Sclerosis (ALS) continue to be major clinical challenges, especially within the elderly demographic.  
 044 (Garofalo et al., 2020). The World Health Organization’s report on Neurological Disorders: Public  
 045 Health Challenges indicates that nearly one billion people worldwide are affected. (Bosco et al.,  
 046 2011). The formidable blood-brain barrier (BBB) continues to pose a major challenge in the ef-  
 047 fective management of neurodegenerative disorders (NDs). The WHO has noted that, despite the  
 048 availability of highly effective and affordable treatments, up to 9 out of 10 individuals with NDs in  
 049 developing countries remain untreated. Enhancing health systems is essential to provide better care  
 050 for those with neurological disorders. Despite ongoing efforts in modern science to develop medical  
 051 or surgical interventions, the results have been largely disappointing. This underscores the critical  
 052 need for further research in this field.

053 Language deficits are frequently observed in numerous neurodegenerative conditions, often emerg-  
 ing early as a prominent symptom. Therefore, identifying and characterizing language impairments

in patients with NDs is becoming increasingly important for diagnosing various neurodegenerative diseases. (Boschi et al., 2017). Furthermore, neurodegenerative disorders can impact speech due to the decline in motor control. Symptoms of PD related to the motor system include tremors, rigidity, poor balance, and slow movement. (Jeong et al., 2024). Specifically, motor speech irregularities associated with PD impact elements such as prosody, resonance, articulation, breathing, and phonation. (Magee et al., 2019). Although the exploration of language-related issues in Amyotrophic Lateral Sclerosis (ALS) has been limited, some studies have highlighted language deficits in ALS patients without dementia, revealing the presence of diverse cognitive profiles. Individuals with ALS may face challenges with articulation and understanding sentence structure, resulting in simplified syntax and difficulties in comprehending complex syntax. This motivates researchers to develop diagnostic assistive speech tools to aid in the classification of various Neurodegenerative Diseases (NDs). The literature predominantly focuses on the classification of PD in comparison to ALS.

## 2 RELATED WORK

In recent decades, there has been increasing interest in automatically identifying neurological diseases through the analysis of vocal recordings. (Benba et al., 2016; Rusz et al., 2011; Orozco-Arroyave et al., 2016). In the study referenced in (Kim, 2017), the authors examine the fricative sounds produced by individuals with Parkinson’s Disease (PD). The study also explores the significance of nasal consonants in the automatic identification of PD. (Spangler et al., 2017). In (Moro-Velazquez et al., 2019), the role of nasal consonants in the automatic identification of individuals with Parkinson’s Disease (PD) was explored. In (Moro-Velazquez et al., 2019), the authors also proposed a method utilizing Perceptual Linear Prediction (PLP) features and Gaussian Mixture Models (GMM) with Universal Background Models (UBM) classifiers for the classification of Healthy vs. PD.

In (Vashkevich & Rushkevich, 2021), various acoustic features such as Jitter, Shimmer, Mel Frequency Cepstral Coefficients (MFCC), Formant Frequencies, and Pitch Period Entropy are used for the classification of Healthy individuals vs. those with neurodegenerative disease based on sustained vowels. Additionally, (Simmatis et al., 2024) also utilized acoustic and articulatory features for ALS classification. However, there is limited research on classifying multiple neurodegenerative diseases simultaneously. The study reported in (Suhas et al., 2020) investigates a Mel-Spectrogram-based approach for distinguishing between Parkinson’s Disease, ALS, and Healthy Controls. Additionally, in the context of Heisenberg’s uncertainty principle applied to signal processing, the Short-Time Fourier Transform (STFT) used in MFCC imposes a fixed time-frequency resolution across the entire time-frequency plane. Moreover, it lacks the *form-invariance* property, as the analysis window in STFT depends exclusively on the *time* parameter (Gambarella, 1968). To that effect, we propose a novel feature extraction method based on the Constant-Q Transform (CQT) and its cepstral representation, known as Constant Q Cepstral Coefficients (CQCC) for classification of Neurodegenerative disorders. Originally introduced in the context of antispoofting literature (Todisco et al., Bilbao, Spain, June 21-24, 2017), CQCC has also demonstrated strong performance in the classification of pathological infant cries (Patil et al., 2023).

- Furthermore, no studies have reported on capturing the neurodegenerative disease on sustained vowel sounds through *Form-Invariance* property of CQT.
- To the best of the authors’ knowledge, this is the first study of its kind on sustained vowel sounds for multi neurodegenerative disorder classification and analysis.

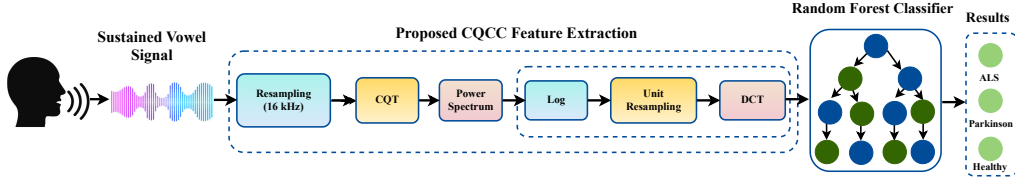


Figure 1: Functional block diagram of proposed CQCC Feature Set for Classification of Neurodegenerative Disorders. After (Patil et al., 2023). Best viewed in colour.

108 Table 1: Window length  $v(m, r)$  in samples as a function of analysis frequency ( $g_r$ ). Adapted from  
 109 (Brown, 1991).

r	Frequency (Hz)	# Samples	Duration (in ms)
1	100	29547	1340
100	204.37	14457	655.64
200	420	7022	318.48
400	1783	1657	75.15
600	7556	391	17.73

### 3 METHODOLOGY

This section discusses about the Constant Q transform (CQT) feature extraction and the *Form-Invariance* property of CQT

#### 3.1 THE CONSTANT-Q TRANSFORM (CQT)

The Discrete Fourier Transform (DFT) is essentially a sampled version of the Discrete-Time Fourier Transform (DTFT) applied to each frame of the speech signal (Brown, 1991). Let  $z(m)$  be the discrete-time input speech signal with a sampling rate of  $F_r$ . The Short-Time Fourier Transform (STFT) of  $z(m)$  is expressed as (Quatieri, 2015):

$$Z(\theta, \mu) = \sum_{m=-\infty}^{\infty} z(m) \cdot v(m, \mu) \cdot e^{-j\theta m}, \quad (1)$$

where  $v(m, \mu)$  denotes the analysis window centered at time  $\mu$ . It is important to note that  $v(m, \mu)$  is a function of only the time variable  $\mu$ . Furthermore, let  $w_p(m) = z(m)v(m, \mu)$  represent a windowed frame of the speech signal, then the  $M$ -point DFT,  $W_p(r)$ , of  $w_p(m)$  can be represented as:

$$W_p(r) = \sum_{m=0}^{M-1} w_p(m) \cdot e^{-j(\frac{2\pi}{M})rm}, \quad (2)$$

where  $r$  is the frequency bin index, and  $\theta_{DFT} = (2\pi r)/M$  (i.e., uniform frequency spacing). In this research, we have employed the CQCC instead of the STFT-based feature sets. The Constant-Q Transform (CQT) offers superior frequency resolution in lower frequency regions. In CQT, the quality factor  $P$  of the subband filters used in the filter bank remains constant (as discussed in eq. (5)), thus leading to geometrically spaced frequency bins as introduced in Brown's original work (Brown, 1991). The CQT of a signal  $w_p(m)$  is given by:

$$W_p^{CQT}(r) = \frac{1}{M(r)} \sum_{r=0}^{M(r)-1} w_p(m)v(m, r)e^{-j\left(\frac{2\pi}{M(r)} P m\right)}, \quad (3)$$

where  $\theta_{CQT} = (2\pi P m)/M(r)$ , and  $v(m, r)$  is the analysis window, which has a consistent shape for the analysis of each frequency component  $g_r$ , though its length is determined by  $M(r)$ , making it a function of both time ( $m$ ) and frequency ( $r$ ), where

$$M(r) = P \left( \frac{F_r}{g_r} \right). \quad (4)$$

It should be observed that  $v(m, \mu)$  in eq. (1) is only a function of the time parameter ' $\mu$ ', whereas  $v(m, r)$  in eq. (3) is a function of both time ( $m$ ) and frequency ( $r$ ). Table 1 displays the window durations for the CQT parameter set in infant cry classification. From Table 1, it can be seen that the window length varies with respect to  $g_r$ , reducing as  $g_r$  increases. The window duration is significantly larger in the lower frequency regions, offering high frequency resolution, making the CQT an effective method to capture infant cry characteristics in lower frequency ranges.

162

**Algorithm 1:** Pseudo-Code of the Revised CQCC Feature Set. Adapted from (Patil et al., 2023).

```

164 1:  $g_m = (2^{\frac{m-1}{D}})g_{min}$  geometrically spaced frequency bins
165 2:  $M(m) = \frac{S_r}{\Delta g_m}$ 
166 3:  $Z_r^{CQT}(m) = \left\langle z_r(p) \cdot \psi(p, m), e^{j \frac{2\pi R_p}{M(m)}} \right\rangle$  computation of CQT for the speech segment  $z_r(m)$ 
167 4: for  $j = 1 : N_{columns}(Z_{CQT})$  do
168 5:   Framewise concatenation of CQT:
169 6:    $Z_{CQT}(m, j) = Z_{z_{rj}}^{CQT}(m)$  CQT computed for the corresponding segment  $z_{r_j}(p)$  for the  $j^{th}$  column
170 7: end for
171 8:  $Z_{CQT}^{resampled}(m, j) = resample(Z_{CQT}(m, j))$  Frequency bins resampled for linear spacing
172 9:  $CQCC = DCT \left( \log \left( Z_{CQT}^{resampled}(m, j) \right) \right)$ 
173
174

```

175

177 Since the quality factor  $P$  is the ratio of center frequency to bandwidth, it is defined as (Brown,  
178 1991):

$$P = \frac{g_r}{\Delta g_r} = \frac{g_r}{q_{r+1} - q_r} = \frac{1}{2^{1/B} - 1}, \quad (5)$$

where  $B$  is the number of bins per octave, and  $g_r$  represents the frequency of the  $r^{th}$  spectral component, as defined by (Brown, 1991):

$$q_r = (2^{(r-1)/B}) q_{min}, \quad (6)$$

where  $g_{min}$  is the minimum frequency of the signal. Additionally, we resampled the magnitude spectrum of the CQT to a linear scale to reduce the number of frequency bins in the feature set (Todisco et al., Bilbao, Spain, June 21-24, 2017). Substituting eq. (5) into eq. (4), we have:

$$M(r) = \frac{F_r}{\Delta G_r}. \quad (7)$$

194 Additionally, we converted the geometrically-spaced frequency scale to a linearly-spaced one to  
 195 maintain the orthogonality of the Discrete Cosine Transform (DCT). Since frequency bins in CQT  
 196 are geometrically spaced, reconstructing the signal can be viewed as a downsampling operation for  
 197 the initial  $r$  bins, corresponding to lower frequencies, and as upsampling for the remaining  $R - r$   
 198 bins, corresponding to higher frequencies. Further details on resampling can be found in (Todisco  
 199 et al., Bilbao, Spain, June 21-24, 2017). Applying the DCT to the resampled CQT produces the  
 200 CQCC feature set. The pseudo-code for CQCC feature extraction is given in Algorithm 1. Figure  
 201 1 outlines the functional block diagram of the proposed CQCC-based neurodegenerative disease  
 classification system.

203 3.1.1 FORM-INvariance PROPERTY OF COT

For simplicity, we examine the continuous-time forms of the Fourier Transform (FT), Short-Time Fourier Transform (STFT), and Constant-Q Transform (CQT). If  $y(t)$  and  $Y(\xi)$  are a Fourier transform pair, then the time-scaling property of the Fourier Transform can be expressed as follows (Gambardella, 1968), (Quatieri, 2015):

$$\mathcal{F}\{y(\beta t)\} = \frac{1}{|\beta|} Y\left(\frac{\xi}{\beta}\right), \quad (8)$$

indicating that scaling the time domain by a factor of  $\beta$  corresponds to scaling the frequency domain by the *inverse* factor  $\frac{1}{\beta}$ . This shows that the structure of the energy spectral density (ESD) remains unchanged, which is why this property is referred to as "form-invariance." However, this property does not extend to the conventional STFT, where the analysis window function depends solely on the time variable.

Schroeder and Atal introduced the STFT using practically realizable bandpass Linear Time-Invariant (LTI) filters (Schroeder & Atal, 1962), defining it as follows:

$$Y(t, \xi) = \int_{-\infty}^t y(\theta) \psi(t - \theta) e^{-j\xi\theta} d\theta. \quad (9)$$

For the STFT to be form-invariant, the following condition must hold:

$$\text{STFT}\{y(lt)\} = Y_l(t, \xi) = \eta Y(\gamma t, \delta \xi), \quad (10)$$

where  $\gamma$  and  $\delta$  represent time and frequency scaling factors, respectively. It has been shown that realizing this condition places necessary and sufficient constraints on the window function, requiring it to belong to a class of single-term power functions:  $\psi(t) = ct^d$ ,  $t > 0$ , where  $c$  and  $d$  are real constants. According to the stability condition for LTI filters, this window is *unstable*, making it impractical for real-world applications.

However, it is interesting to note that the situation changes if the window function depends on both time and frequency, i.e.,  $\psi(t) \equiv \psi(t, \xi)$ , as in the case of CQT. In this scenario, the STFT equation becomes the following:

$$Y(t, \xi) = \int_{-\infty}^t y(\theta) \psi(t - \theta, \xi) e^{-j\xi\theta} d\theta, \quad (11)$$

and the form-invariance condition is satisfied for the window function. Further technical details of this condition are provided in the Appendix. Specifically, the window function takes the following form:

$$\psi(t, \xi) = cv(t\xi)t^d, \quad t > 0, l > 0, \xi > 0, \quad (12)$$

where  $v(t\xi)$  is an arbitrary real function of  $t\xi$ , and  $c$  and  $d$  are real constants. Furthermore,  $\psi(t, \xi)$  also adheres to the Bounded Input and Bounded Output (BIBO) stability conditions for an LTI filter, meaning that its impulse response is absolutely integrable (Oppenheim et al., 2001), as expressed in the following condition:

$$\int_{-\infty}^{+\infty} |\psi(t, \xi)| dt < \infty. \quad (13)$$

Moreover, this form of the window function applies to practical models involving short-time analysis, such as those that mimic the auditory system's peripheral processing. For example, Flanagan's original model (Flanagan, 2013) describes the window function used in mechanical spectral analysis due to the movements of the basilar membrane in the cochlea of the human ear (Gambardella, 1968). In particular, the window function is given by  $\psi(t, \xi) = (t\xi)^2 e^{-\frac{t\xi}{2}}$ , which is similar to the form described above.

## 4 EXPERIMENTAL SETUP

### 4.1 DATASETS DETAILS

In this study, we use Italian Parkinson's Voice and Speech dataset, which was designed in association with "Associazione Parkinson Puglia" (Dimauro & Girardi, 2019). Additionally, we also used Minsk2019 ALS database which was designed using recordings made from Republican Research and Clinical Center of Neurology and Neurosurgery (Minsk, Bela) (Vashkevich et al., 2019). Both dataset contains the sustained sounds of all vowel sounds. Since the sampling rate of the cry signals provided in the dataset is not uniform, we resampled all the utterances at a sampling rate of 16 kHz. The dataset consists of sustained vowel phonations from individuals diagnosed with Parkinson and ALS along with healthy controls at a comfortable pitch and loudness as constant and long as possible. The imbalance in dataset was handled using *SMOTE*. For training and testing, we used 80% and 20% of the data, respectively. Table 2 shows the statistics of all datasets utilized. Further, 3, shows the agewise distribution of parkinson patients and healthy controls in the Italian Parkinson Dataset.

270 Table 2: Statistics of the Italian Parkinson’s and Minsk2019 ALS database used. After (Dimauro &  
 271 Girardi, 2019; Vashkevich et al., 2019).

<b>Class →</b>	<b>Healthy</b>	<b>Pathology</b>	
<b>Dataset↓</b>		<b>PD</b>	<b>ALS</b>
<b>D1</b>	220	220	77
<b>D2</b>	220		297
<b>D3</b>	-	100	77

278  
 279 Table 3: Participant Distribution in the Italian Parkinson’s Dataset  
 280

<b>Group</b>	<b>Subgroup</b>	<b>Age Range (Years)</b>	<b>Male (M)</b>	<b>Female (F)</b>	<b>Total</b>
Parkinson’s	Young	19–45	4	2	6
	Old	50+	19	9	28
Healthy	Young	19–45	4	2	6
	Old	50+	10	12	22
Total			37	25	62

#### 288 4.2 CLASSIFIER USED

290 The experiments were carried out using the Random Forest (RF) classifier with 100 nestimators and  
 291 random state of 42, which is commonly used for the classification of neurodegenerative diseases. In  
 292 this study, we also employ the Support Vector Machine (SVM) with *RBF* kernel and  $c = 1$ .

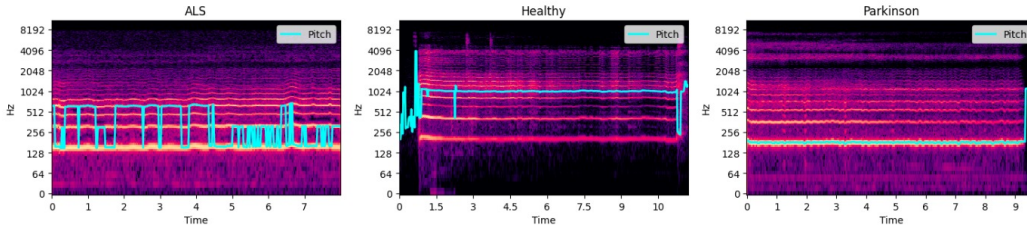
293 **Evaluation Metrics:** Performance of all systems is evaluated using % classification accuracy

#### 295 4.3 FEATURE SETS USED

297 In this study, the performance of the proposed Constant Q Cepstral Coefficients (CQCC) and its  
 298 components is compared with state-of-the-art MFCC features, as well as Jitter, Shimmer, and Teager  
 299 Energy, serving as baseline features. The baseline MFCC features were extracted from the audio  
 300 files at a fixed sample rate of 16 kHz, with a window length of 512 samples and a window shift of  
 301 256 samples. For the CQCC feature extraction, a minimum frequency ( $f_{\min}$ ) of 20 Hz was set, and  
 302 a total of 20 CQCC coefficients were extracted to evaluate the performance against a total of 13  
 303 MFCC coefficients.

### 304 5 EXPERIMENTAL DISCUSSION

#### 306 5.1 SPECTROGRAPHIC ANALYSIS



317 Figure 2: Spectrographic Analysis and Pitch Contours for Various Disorders Best viewed in colour.  
 318

319 Key regions affected include the corticospinal tract and the motor cortex. The degeneration in these  
 320 areas results in impaired voluntary muscle movements, which manifest as the observed instability  
 321 and interruptions in phonation in ALS patients. As observed from Figure 2(a), the spectrogram  
 322 of an ALS patient demonstrates irregular and sporadic pitch contours with significant frequency  
 323 fluctuations. The instability in pitch is indicative of the muscle weakness and severe effect on vocal  
 cord control. The frequent breaks and variations in the pitch contour reflect the effortful and strained

nature of speech in ALS patients. ALS impacts the motor neurons in both the brain and spinal cord, leading to muscle weakness and spasticity. Additionally, the harmonic structure in the ALS spectrogram appears less regular and more fragmented, which mirrors the effortful and strained nature of speech. This irregularity arises from inconsistent vocal fold vibrations due to impaired muscle control. Temporal patterns in the ALS spectrogram may show uneven or interrupted speech segments, reflecting the effortful and strained nature of their speech production.

In contrast, the spectrogram of a healthy individual, as illustrated in Figure 2(b), exhibits a stable and consistent pitch contour. The formant frequencies, represented by the horizontal bands, are well-defined and continuous over time. This stability and clarity in the spectral features are typical of normal phonation, where the vocal cords vibrate regularly and smoothly, producing a steady pitch. Healthy individuals have intact motor neuron function and brain structures, which allow for precise control over the vocal apparatus. The harmonic structure in healthy individuals is regular and well-defined, indicating smooth and consistent vocal fold vibrations. Temporal patterns are regular and continuous, indicative of fluent and effortless speech.

Parkinson’s disease primarily affects the substantia nigra in the basal ganglia, leading to dopamine deficiency and resulting in impaired motor control and reduced vocal cord movement. As observed from Figure 2(c), the spectrogram of a Parkinson’s patient reveals a relatively stable but low-pitched contour compared to the healthy individual. The pitch contour is more monotone, reflecting the characteristic of Parkinson’s disease. This monotonic pitch, along with reduced amplitude modulation, results from the reduced range and control of vocal cord movements in Parkinson’s patients. The harmonic structure in Parkinson’s patients may show reduced harmonic energy and lower overall intensity, reflecting the softer and more monotone speech pattern. Temporal patterns in Parkinson’s patients may show prolonged phonation of certain sounds and a reduced speech rate, contributing to their overall monotone speech.

## 5.2 EXPERIMENTAL RESULTS AND DISCUSSION

This section discusses the overall performance of proposed CQCC feature against baseline features. Further, it also discusses about the spectrographic analysis between different neurodegenerative disorders and finally, LDA plots are analyzed for better feature visualizations.

### 5.2.1 OVERALL PERFORMANCE FOR BINARY CLASSIFICATION

In this subsection, we discuss the results obtained on binary classification for healthy *vs.* pathological speech for database **D2** considered in this work. Table 4 reports the accuracy obtained on both classifiers for all the features sets considered in this study.

Table 4: Classification Accuracy of RF and SVM for Different Features

Classifier	Jitter	Shimmer	Teager Energy	MFCC	CQCC
RF Accuracy (%)	63.4	62.9	65.3	95.1	99.0
SVM Accuracy (%)	53.8	65.3	62.5	88.4	63.4

As observed from Table 4, it can be observed that, Among the features analyzed, CQCC achieved the highest classification accuracy, with the Random Forest classifier attaining an exceptional 99%, in contrast to the 63.4% accuracy achieved by the Support Vector Machine classifier. CQCC excels due to its sophisticated time-frequency representation, which captures subtle and intricate spectral variations essential for distinguishing pathological speech from healthy speech. This feature’s detailed depiction of temporal and frequency characteristics enables the RF classifier to effectively discern and leverage complex patterns indicative of pathological conditions. The superior performance of RF with CQCC underscores its ability to handle and interpret the nuanced information provided by this feature. This suggests that CQCC, combined with RF’s advanced classification capabilities, provides a robust framework for identifying subtle speech abnormalities with high precision.

### 5.2.2 CLASSIFICATION BETWEEN DIFFERENT PATHOLOGIES

As studied in section 5.2.1, it was observed that CQCC outperformed the MFCC, Jitter, Shimmer, and Teager energy feature sets for the classification of healthy versus pathological sounds. Here, we

378  
379  
Table 5: Classification Accuracy of RF and SVM for Different Features  
380  
381  
382

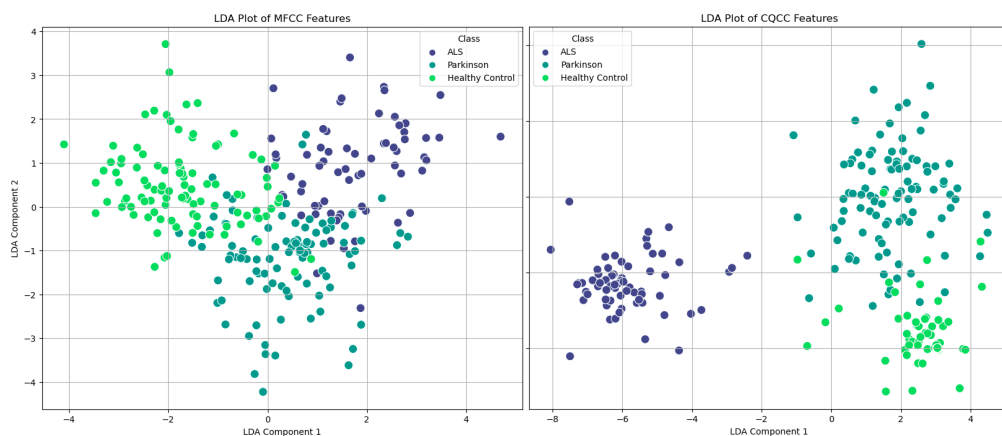
Classifier	Jitter	Shimmer	Teager Energy	MFCC	CQCC
RF Accuracy (%)	41.6	57.6	49.6	84.6	90.3
SVM Accuracy (%)	44.2	50.9	44.2	73.0	80.7

383  
384  
385 discuss the results obtained on multiple pathological classifications. Two new databases **D1** and **D3**  
386 were prepared, where two different pathologies, along with healthy controls from both databases,  
387 were considered. Table 5 reports the results on baseline as well as proposed feature sets using  
388 RF and SVM as classifiers. It can be observed from the tables that the proposed CQCC features  
389 outperform the baseline MFCC features with an absolute increment of 5.6% and 7.7% on RF and  
390 SVM classifiers, respectively. To that effectm it can be observed that CQCC has ability to provide  
391 a comprehensive depiction of both temporal and frequency characteristics enables RF to effectively  
392 discern and leverage the complex patterns indicative of these conditions.

393  
Table 6: Classification Accuracy of RF and SVM for Different Features  
394

Classifier	Jitter	Shimmer	Teager Energy	MFCC	CQCC
RF Accuracy (%)	63.8	69.4	66.6	80.5	80.5
SVM Accuracy (%)	52.7	69.4	63.8	63.8	86.1

395 Furthermore, Table 6, shows the classification results between ALS and Parkinson’s patients across  
396 different acoustical features when employing Random Forest (RF) and Support Vector Machine  
397 (SVM) classifiers. It can be observed from Table 6 that CQCC yields the highest accuracy with  
398 SVM (86.1%) and consistently performs well with RF (80.5%), indicating its superior capability in  
399 capturing the nuanced differences in the vocal characteristics associated with these diseases. On the  
400 other hand, features like Jitter and Shimmer show relatively lower accuracies, particularly with SVM  
401 (52.7% and 69.4% respectively), highlighting that these perturbation measures might not capture  
402 the disease-specific vocal characteristics as effectively. Teager Energy and MFCC (Mel Frequency  
403 Cepstral Coefficients) also show moderate performance, indicating their utility but not as robust as  
404 CQCC.  
405

406  
5.2.3 FEATURE VISULIZATION USING LDA PLOTS  
407408  
Figure 3: LDA plots for MFCC and CQCC features showing improved class separation with CQCC.  
409 Best viewed in colour.  
410

411 The LDA plot as shown in Figure 3, MFCC features reveals a moderate overlap between the three  
412 classes. ALS and Parkinson’s disease samples display a slight separation along the first LDA com-  
413 ponent, with Parkinson’s samples tending to cluster more closely in a specific region, while ALS  
414 shows broader dispersion. Healthy Control samples, although overlapping with ALS and Parkinson,

are more distinguishable, particularly in the negative region of the first component. This moderate separability suggests that while MFCC captures useful information related to voice characteristics, it may not be fully sufficient for high-accuracy classification of the three groups. However, the LDA plot of CQCC features exhibits a clearer separation, especially between the ALS and Parkinson’s disease classes. ALS samples are tightly clustered on the far left, showing a distinct separation from the Parkinson and Healthy Control classes. Healthy Control samples are spread across a different region, especially in the positive range of the first LDA component, indicating less overlap with Parkinson’s disease samples. This stronger discriminative power indicates that CQCC features are more effective at distinguishing between neurodegenerative disorders and healthy individuals, making them a more robust feature set for classification tasks.

## 6 CONCLUSIONS

This study comprehensively assessed various characteristics to distinguish between healthy and pathological speech using SVM and RF classifiers. The findings underscore that CQCCs emerged as the most effective feature, achieving the highest accuracy in classification tasks. Particularly notable was RF’s performance, significantly outperforming SVM, which highlights RF’s capability in leveraging intricate time-frequency representations inherent in CQCC. It also demonstrated substantial efficacy, surpassing traditional measures such as Jitter, Shimmer, and Teager Energy in accuracy. This underscores the relevance of the quality features of the cepstral to accurately identify pathological speech conditions. Comparison with MFCC further validated the superiority of CQCC, showing considerable improvements in both the RF and SVM classifiers. Furthermore, the evaluation in new databases (D1 and D3) reaffirmed the robustness of CQCC in handling complex pathological classifications, providing further validation of their utility in clinical applications. Future research directions should focus on validating these findings in diverse pathological datasets and exploring advanced machine learning techniques to further improve classification precision.

## REFERENCES

- Achraf Benba, Abdelilah Jilbab, and Ahmed Hammouch. Discriminating between patients with parkinson’s and neurological diseases using cepstral analysis. *IEEE transactions on neural systems and rehabilitation engineering*, 24(10):1100–1108, 2016.
- Veronica Boschi, Eleonora Catricala, Monica Consonni, Cristiano Chesi, Andrea Moro, and Stefano F Cappa. Connected speech in neurodegenerative language disorders: a review. *Frontiers in psychology*, 8:269, 2017.
- Daryl A Bosco, Matthew J LaVoie, Gregory A Petsko, and Dagmar Ringe. Proteostasis and movement disorders: Parkinson’s disease and amyotrophic lateral sclerosis. *Cold Spring Harbor perspectives in biology*, 3(10):a007500, 2011.
- Judith C. Brown. Calculation of a constant Q spectral transform. *The Journal of the Acoustical Society of America (JASA)*, 89(1):425–434, 1991.
- Giovanni Dimauro and Francesco Girardi. Italian parkinson’s voice and speech, 2019. URL <https://dx.doi.org/10.21227/aw6b-tg17>.
- James L. Flanagan. *Speech analysis synthesis and perception*, volume 3. Springer Science & Business Media, 2013.
- G. Gambardella. Time scaling and short-time spectral analysis. *The Journal of the Acoustical Society of America (JASA)*, 44(6):1745–1747, 1968.
- Maria Garofalo, Cecilia Pandini, Matteo Bordoni, Orietta Pansarasa, Federica Rey, Alfredo Costa, Brigida Minafra, Luca Diamanti, Susanna Zucca, Stephana Carelli, et al. Alzheimer’s, parkinson’s disease and amyotrophic lateral sclerosis gene expression patterns divergence reveals different grade of rna metabolism involvement. *International Journal of Molecular Sciences*, 21(24):9500, 2020.

- 486 Seung-Min Jeong, Seunghyun Kim, Eui Chul Lee, and Han Joon Kim. Exploring spectrogram-  
 487 based audio classification for parkinson's disease: A study on speech classification and qualitative  
 488 reliability verification. *Sensors*, 24(14):4625, 2024.
- 489
- 490 Yunjung Kim. Acoustic characteristics of fricatives/s/and//produced by speakers with parkinson's  
 491 disease. *Clinical archives of communication disorders*, 2(1):7, 2017.
- 492 Michelle Magee, David Copland, and Adam P Vogel. Motor speech and non-motor language en-  
 493 dophenotypes of parkinson's disease. *Expert Review of Neurotherapeutics*, 19(12):1191–1200,  
 494 2019.
- 495
- 496 Laureano Moro-Velazquez, Jorge A Gomez-Garcia, Juan I Godino-Llorente, Francisco Grandas-  
 497 Perez, Stefanie Shattuck-Hufnagel, Virginia Yagüe-Jimenez, and Najim Dehak. Phonetic rele-  
 498 vance and phonemic grouping of speech in the automatic detection of parkinson's disease. *Sci-  
 499 entific reports*, 9(1):19066, 2019.
- 500 Alan V Oppenheim, John R Buck, and Ronald W Schafer. *Discrete-Time Signal Processing*. Vol. 2.  
 501 Upper Saddle River, NJ: Prentice Hall, 2001.
- 502 Juan Rafael Orozco-Arroyave, F Hönig, JD Arias-Londoño, JF Vargas-Bonilla, K Daqrouq,  
 503 S Skodda, J Rusz, and E Nöth. Automatic detection of parkinson's disease in running speech  
 504 spoken in three different languages. *The Journal of the Acoustical Society of America*, 139(1):  
 505 481–500, 2016.
- 506
- 507 Hemant A. Patil, Aastha Kachhi, and Ankur T. Patil. Cqt-based cepstral features for classification  
 508 of normal vs. pathological infant cry. *IEEE/ACM Transactions on Audio, Speech, and Language  
 509 Processing*, pp. 1–14, 2023. doi: 10.1109/TASLP.2023.3325971.
- 510 Thomas F. Quatieri. *Discrete-Time Speech Signal Processing: Principles and Practice*. 1<sup>st</sup> Edition,  
 511 Pearson Education India, 2015.
- 512
- 513 Jan Rusz, Roman Cmejla, Hana Ruzickova, and Evzen Ruzicka. Quantitative acoustic measurements  
 514 for characterization of speech and voice disorders in early untreated parkinson's disease. *The  
 515 journal of the Acoustical Society of America*, 129(1):350–367, 2011.
- 516 Manfred R. Schroeder and Bishnu S. Atal. Generalized short-time power spectra and autocorrelation  
 517 functions. *The Journal of the Acoustical Society of America (JASA)*, 34(11):1679–1683, 1962.
- 518
- 519 Leif ER Simmatis, Jessica Robin, Michael J Spilka, and Yana Yunusova. Detecting bulbar amy-  
 520 otrophic lateral sclerosis (als) using automatic acoustic analysis. *BioMedical Engineering On-  
 521 Line*, 23(1):15, 2024.
- 522 Taylor Spangler, NV Vinodchandran, Ashok Samal, and Jordan R Green. Fractal features for au-  
 523 tomatic detection of dysarthria. In *2017 IEEE EMBS international conference on biomedical &  
 524 health informatics (BHI)*, pp. 437–440. IEEE, 2017.
- 525
- 526 BN Suhas, Jhansi Mallela, Aravind Illa, BK Yamini, Nalini Atchayaram, Ravi Yadav, Dipanjan  
 527 Gope, and Prasanta Kumar Ghosh. Speech task based automatic classification of als and parkin-  
 528 son's disease and their severity using log mel spectrograms. In *2020 international conference on  
 529 signal processing and communications (SPCOM)*, pp. 1–5. IEEE, 2020.
- 530
- 531 Massimiliano Todisco, Héctor Delgado, and Nicholas Evans. Constant-Q cepstral coefficients: A  
 532 spoofing countermeasure for automatic speaker verification. *Computer Speech & Language*, 2017  
*Bilbao, Spain*, 45:516–535, Bilbao, Spain, June 21-24, 2017.
- 533
- 534 Maxim Vashkevich and Yu Rushkevich. Classification of als patients based on acoustic analysis of  
 535 sustained vowel phonations. *Biomedical Signal Processing and Control*, 65:102350, 2021.
- 536
- 537 Maxim Vashkevich, Alexander Petrovsky, and Yuliya Rushkevich. Bulbar als detection based on  
 538 analysis of voice perturbation and vibrato. In *2019 Signal Processing: Algorithms, Architectures,  
 Arrangements, and Applications (SPA)*, pp. 267–272. IEEE, 2019.
- 539